



Cite this: *Dalton Trans.*, 2024, **53**, 18069

Recent advances in tailoring the microenvironment of Pd-based catalysts for enhancing the performance in the direct synthesis of hydrogen peroxide

Ying Zhang,^a Xilun Wang,^a Ziyue Wang,^a Liyang Liu,^a Xiaohui He ^{*a,c} and Hongbing Ji ^{*a,b}

Hydrogen peroxide (H₂O₂) is a valuable clean chemical, which is widely applied in modern industrial production. In the past few decades, H₂O₂ has been mainly produced industrially by the anthraquinone method, but the process is complicated and energy consuming, which is only economical for large-scale production and is harmful to the environment. The direct synthesis of H₂O₂ is considered a promising process to replace the anthraquinone method with high atomic economy, no hazardous by-products, and convenient operation, which has attracted much attention. In this review, we systematically present the recent advances in tuning the microenvironment of Pd-based catalysts for enhancing the performance of the direct synthesis of H₂O₂, including the modulation of active sites and support, from the viewpoint of the reaction mechanism. Finally, a summary and perspective on the most pressing issues and associated untapped research prospects with the direct synthesis of H₂O₂ are discussed. The purpose of this review is to provide in-depth insights and guidelines to promote the development of novel catalysts for the direct synthesis of H₂O₂.

Received 29th August 2024,
Accepted 30th September 2024

DOI: 10.1039/d4dt02460e

rsc.li/dalton

Introduction

Hydrogen peroxide (H₂O₂), an important clean and environmentally friendly chemical with an annual output value of more than \$4 billion, was found in 1818 by Thenard as a product of the reaction between barium peroxide and nitric acid.^{1,2} As a strong oxidant, H₂O is the only by-product, which makes H₂O₂ widely used in various fields.^{3–5} Typically, H₂O₂ in concentrations of 3–5 wt% is used for sterilization in household, medical, dental, and cosmetic products. Concentrations of up to 70 wt% are employed in chemical synthesis, wastewater treatment, mining, and bleaching.⁶ Higher concentrations of H₂O₂ (70–90 wt%) are employed in the electronics industry for cleaning and corrosion protection, and 90–98 wt% concentrations of H₂O₂ are used in military and aerospace applications.⁷ It is expected that the global production of hydrogen peroxide will reach 5.7 million

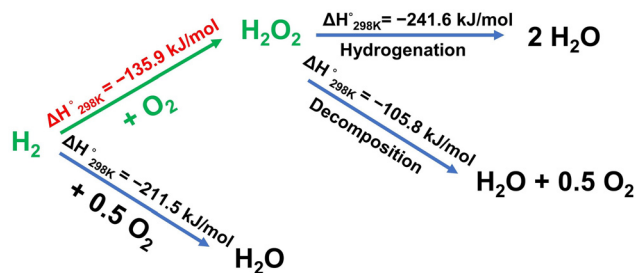
tons by 2027, capturing huge market potential.⁸ Nowadays, over 95% H₂O₂ is mainly produced by the anthraquinone method commercially, involving continuous hydrogenation and oxidation reactions.^{9,10} However, the process not only requires a high investment cost for equipment, but also generates a large amount of hazardous organic compounds, which is inconsistent with the concepts of social development.^{3,11,12} Meanwhile, with the increasing demand for H₂O₂ in recent years, the development of novel eco-friendly and effective methods for H₂O₂ production has become urgent, such as electrochemical synthesis, photocatalytic synthesis, direct synthesis of H₂O₂ (DSHP), *etc.*^{5,13}

Considering the extensive organic sacrificial agents used and low production efficiency in photocatalysis, as well as the complicated equipment and high energy consumption in electrocatalysis, both of them are far from being able to meet the requirements of industrial production.^{5,13–15} In recent years, the DSHP from molecular H₂ and O₂ has attracted a great deal of attention from numerous researchers, which is considered to be the most promising novel route for the industrial production of H₂O₂ since it not only features a low-cost and environmentally friendly process, but also can be easily integrated with downstream processes and distributed manufacturing.¹⁶ Theoretically, the DSHP process is the simplest and most efficient method available, with 100% atomic economy.¹⁷ However, a number of challenges have been raised, including the complexity of the gas–solid–liquid three-phase reaction

^aKey Laboratory of Bioinorganic and Synthetic Chemistry of Ministry of Education, Fine Chemical Industry Research Institute, School of Chemistry, IGCME, Sun Yat-Sen University, Guangzhou 510275, China. E-mail: jihb@mail.sysu.edu.cn, hexiaohui@mail.sysu.edu.cn

^bState Key Laboratory Breeding Base of Green-Chemical Synthesis Technology, Institute of Green Petroleum Processing and Light Hydrocarbon Conversion, College of Chemical Engineering, Zhejiang University of Technology, Hangzhou, 310014, P. R. China

^cGuangdong Technology Research Center for Synthesis and Separation of Thermosensitive Chemicals, Guangzhou 510275, China



Scheme 1 Reactions and corresponding enthalpies in the direct synthesis of H_2O_2 .¹⁹

with mass transfer limitations and considerable safety issues with a wide explosion range of 4% H_2 –94% H_2 , together with the thermodynamically favorable side reactions shown in Scheme 1, including the dissociation of O_2 to form H_2O ($\text{H}_2 + \text{O}_2 \rightarrow \text{H}_2\text{O}$, $\Delta H_{298\text{K}}^\circ = -211.5 \text{ kJ mol}^{-1}$), H_2O_2 hydrogenation ($\text{H}_2\text{O}_2 + \text{H}_2 \rightarrow 2\text{H}_2\text{O}$, $\Delta H_{298\text{K}}^\circ = -241.6 \text{ kJ mol}^{-1}$), and decomposition ($\text{H}_2\text{O}_2 \rightarrow \text{H}_2\text{O} + 0.5\text{O}_2$, $\Delta H_{298\text{K}}^\circ = -105.8 \text{ kJ mol}^{-1}$) to form H_2O , which results in poor yield, selectivity, and H_2O_2 concentrations.^{4,18,19} Therefore, designing and developing efficient catalysts to inhibit side reactions, especially to avoid irreversible O–O bond breaking that produces H_2O , is an extremely critical step for achieving green production of H_2O_2 in the DSHP.

Pd has been considered an extremely active component in the DSHP owing to its superior capacity to activate hydrogen and oxygen at low operating temperatures compared to other transition metals.²⁰ However, although Pd-based catalysts showed strong catalytic activity in the DSHP, they were also very active in H_2O_2 decomposition and hydrogenation reactions, which led to low H_2O_2 selectivity and productivity, limiting their further industrial applications. Under such circumstances, Pd-based catalysts with appropriate modifications are expected to enhance the selectivity and activity of H_2O_2 in a balanced manner.

Herein, we review the latest advances in the DSHP from the perspective of H_2O_2 production pathways. Starting with the fundamental principles of the reaction, we provide a brief overview of the main reaction pathways, density functional theory (DFT) calculation and reaction media, and then we discuss the recent strategies for enhancing the DSHP performance through catalyst microenvironment modulation in detail. Finally, we point out the current challenges and outlook on the future direction of this topic. This review aims to offer in-depth insights and guidance for researchers interested in innovative green technologies for H_2O_2 synthesis.

Catalytic mechanism

Reaction pathway

As aforementioned, the process of DSHP is susceptible to thermodynamically favored side reactions, which can cause low H_2O_2 selectivity and yields. In general, it is recognized that

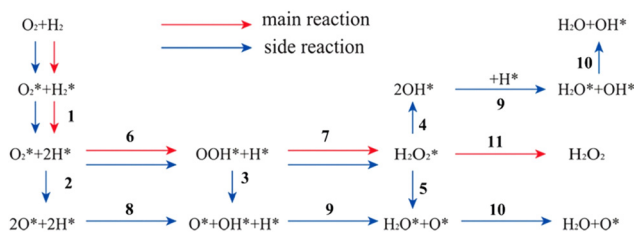


Fig. 1 Schematic diagram of all elementary steps in the reaction network for the direct synthesis of H_2O_2 .²¹

the DSHP reaction pathway is a two-step hydrogenation process of molecular O_2 .²¹ As shown in Fig. 1, molecular H_2 and O_2 are introduced and adsorbed on the active sites, after which the adsorbed *H_2 ($*$ represents adsorption) is dissociated (the H–H bond is broken) to produce two *H , while at the same time O_2 is adsorbed only without dissociation (*O_2 , the O–O bond is not broken, pathway 1). Subsequently, the *O_2 combines with one of the *H to form *OOH (pathway 6), a key intermediate for H_2O_2 production. Finally, *OOH forms $\text{*H}_2\text{O}_2$ with the remaining *H (pathway 7) and desorbs from the active sites to form H_2O_2 (pathway 11). However, there are a few points that need serious attention in the above process: (1) *O_2 is easily activated to form *O (pathway 2); (2) the O–O bond in *OOH adsorbed on the catalyst surface is unstable and easily breaks to form *O and *OH (pathway 3), whereby *OH reacts with *H to form water (pathway 9); (3) the O–O bonds in the generated $\text{*H}_2\text{O}_2$ are susceptible to decomposition (pathways 5 and 10) or hydrogenation (pathways 4, 9, and 10) in the presence of a Pd-based catalyst to form H_2O . Therefore, how to inhibit the occurrence of the mentioned issues is a great challenge for the future design of high-efficiency DSHP catalysts.

DFT calculation

DFT calculation is a quantum mechanical method for investigating multi-electronic systems and electronic structures, which is commonly used to reveal the dynamic process of reactant molecules on the catalyst surface, helping researchers to give a deeper understanding of the reaction mechanism. Particularly, Han *et al.*²² investigated the size effects of Pd sites ranging from subnano clusters to extended surfaces on DSHP using DFT calculations (Fig. 2). They constructed the Pd cluster models of Pd_{19} , Pd_{38} , and Pd_{55} with Pd(111) and Pd(100) extended surfaces. They found that the coordination and geometry structure seriously affected the Pd catalyst performance. The low-coordinated Pd clusters exhibited higher activities and lower H_2O_2 selectivity compared to high-coordinated Pd extended surfaces. This was primarily because low-coordinated Pd clusters transfer more electrons to adsorbed O_2 revealed by Bader charge analysis, leading to undesired O_2 dissociation. For the Pd sites with similar geometric structures, those with higher coordination numbers displayed superior performance. On the other hand, compared with the similar sizes of Pd clusters, the terrace sites with Pd(100) performed

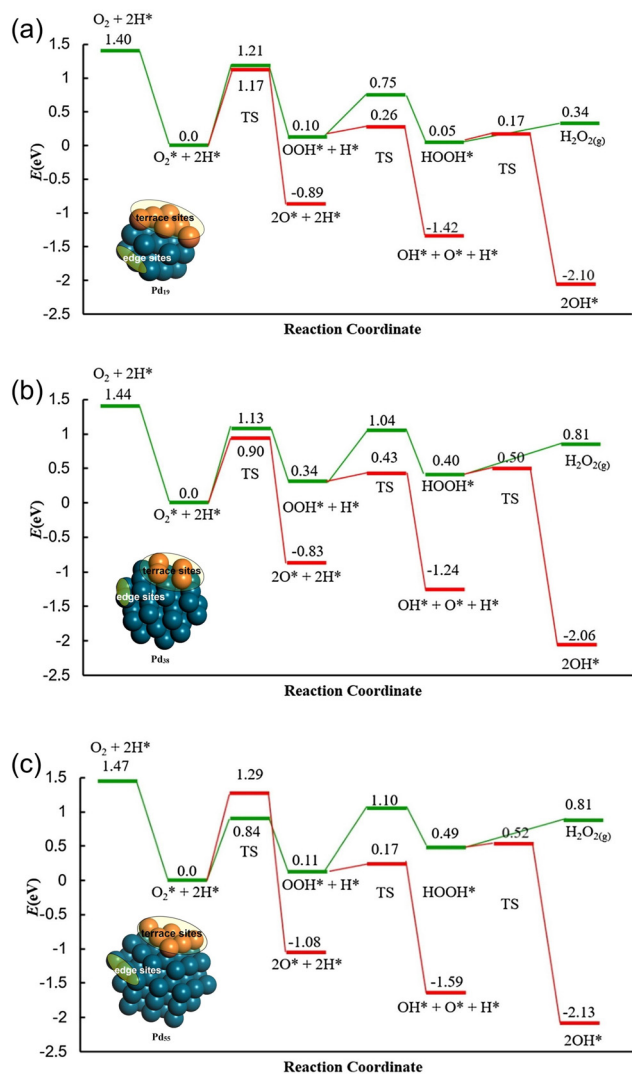


Fig. 2 Pd cluster models and energy diagram for the synthesis of H₂O₂ on edge sites. (a) Pd19 edge, (b) Pd38 edge, and (c) Pd55 edge. The main reactions and side reactions are shown in green and red, respectively.²²

worse than those with Pd(111). However, the results based on the advanced microkinetic modelling by Wang *et al.*²³ suggested that Pd(100), with O₂ and H as the main adsorbates, was more favourable for H₂O₂ formation. Furthermore, Hutchings *et al.*²⁴ have investigated whether the Langmuir-Hinshelwood or electron-proton-transfer mechanism was thermodynamically preferred for DSHP using DFT calculation. They found that both mechanisms were possible, but the electron-proton-transfer mechanism may be more suitable under formal experimental conditions. The above works indicated that DFT calculations can be a useful tool for catalyst design and also can provide an effective approach for a more in-depth insight into reaction mechanisms in DSHP.

Reaction medium

DSHP being a three-phase reaction, the selection of solvent and/or addition of a promoter dramatically affects the reaction

rate as well as the selectivity to H₂O₂. Particularly, H₂O₂ is extremely unstable under alkaline conditions and catalyzed by impurities with active sites, so many reactions are preferred to be carried out under acidic conditions. Hutchings *et al.*²⁵ have prepared PdAu bimetallic catalysts supported on magnesium oxide and carbon, and then systematically investigated the effects of acid additives (H₃PO₄, HNO₃) on the behavior of DSHP. They have found that the acid could significantly decrease the ability of H₂O₂ hydrogenation and decomposition, most notably on magnesium oxide-supported catalysts, whereas for carbon-supported catalysts, it is necessary to optimize the DSHP process by finely controlling the pH (the amount of acid added). Han *et al.*²⁶ suggested that the H₂SO₄/ethanol system is most conducive to the formation of peroxides, while the H₂SO₄/H₂O system serves as a poor medium. This may be due to the formation of acetate ions when ethanol is added, which can coordinate with Pd, thereby inhibiting the generation of H₂O.

It is generally thought that halide ions (Cl⁻, Br⁻) can promote the performance of the DSHP reaction, primarily because halide ions can form corresponding complexes with Pd.^{27,28} Particularly in the case of HCl, H⁺ can inhibit H₂O₂ hydrogenation, while Cl⁻ inhibits the direct reduction of O₂ to water by coordinating with Pd clusters to form PdCl₄²⁻.²⁶ However, acids and halide ions not only corrode equipment, but also pose a challenge for the purification of H₂O₂. Many researchers have used CO₂ as a promoter,²⁹⁻³¹ dissolved in a solvent under reaction conditions, to form carbonic acid (H₂CO₃), which increases the stability of H₂O₂ in the DSHP reaction, being the identical effect achieved by the addition of acids with the same pH. In addition, CO₂ can be degassed and recovered from the solution during depressurization, so it is considered a green promoter for DSHP.³²

The solubility of H₂ and O₂ in the solvent also affects the DSHP performance, so the choice of solvents is also critical. Nijhuis *et al.*³³ systematically investigated the role of water non-miscible co-solvents (1-pentanol, chloroform, hexane, methyl isobutyl ketone), water miscible protic solvents (2-butanol, 1-butanol, i-propanol, methanol, ethanol), and water miscible aprotic solvents (DMSO, acetonitrile, acetone, *t*-butanol) in DSHP. They found that water miscible solvents were more favourable for H₂O₂ production and solvents with lower alcohols showed higher selectivity at moderate to high conversions. Protic solvents also favour the H₂O₂ generation due to the acceleration of the elemental reaction steps (OOH* + H* → H₂O*, OOH* + H* → H₂O + O*) by the protonic H⁺, in agreement with Flaherty's reports.³⁴ Therefore, a mixture of water and methanol is always used as the reaction solvent in the majority of works, because methanol not only acts as a protonic H⁺ donor, but also exhibits high solubility for both H₂ and O₂, thereby reducing mass transfer resistance. However, methanol is a flammable solvent and the cost of separation is so large, presenting significant safety and economic challenges. To solve these problems, Pashkova *et al.*³⁵ employed supercritical CO₂ as a solvent with high solubility of H₂ and O₂ and easy separation of H₂O₂, obtaining 70% H₂O₂ selectivity

and $3.9 \text{ mol g}_{\text{Pd}}^{-1} \text{ h}^{-1}$ H_2O_2 productivity, but there is still much potential for improvement in selectivity and productivity.

Microenvironment modulation strategies on Pd active sites

Valence of active sites

The catalyst is crucial for the DSHP process. The catalyst with Pd as the active component is currently recognized as the most effective. However, there is still no conclusion regarding whether Pd^0 or PdO is more favorable for the formation of H_2O_2 . Choudhary *et al.*³⁶ suggested that Pd^0 was more favorable for H_2 conversion, whereas it also increased the activity for the H_2O_2 decomposition by an order of magnitude. In contrast, PdO demonstrated a significantly high selectivity for H_2O_2 , resulting in a higher yield. Chen *et al.*³⁷ successfully synthesized TiO_2 -supported O-Pd (palladium oxide) catalysts using a hydrothermal method (Fig. 3). Aberration-corrected high-angle annular dark-field scanning transmission electron microscopy (AC HAADF-STEM) revealed that the individual Pd atoms were uniformly distributed on the TiO_2 surface, and the X-ray absorption spectroscopy results confirmed that the Pd atoms were in the oxidized state. This unique Pd-O single-atom structure exhibited superior activity ($>99\%$ H_2O_2 selectivity and $115 \text{ mol g}_{\text{Pd}}^{-1} \text{ h}^{-1}$ H_2O_2 productivity) in the DSHP reaction. Mechanistic studies indicated that Pd single-atom catalysts promoted the formation of key *OOH intermediates and H_2O_2 , while strongly inhibiting the cleavage of O-O bonds in O_2 , *OOH, and H_2O_2 . However, d'Angelo³⁸ and Lunsford³⁹

et al. proposed that Pd^0 is more favorable for the generation of H_2O_2 , followed by partially reduced PdO . Overall, due to the sensitivity of the DSHP reaction to Pd species, the activation abilities of Pd valence for H_2 , O_2 , and H_2O_2 in different systems should be systematically considered for catalyst design in the future. This will lead to a deeper understanding of the specific active sites of Pd species.

Crystal facet regulation

The crystal-facet structure of Pd can significantly affect the adsorption and activation of reactants, ultimately impacting the reaction kinetics and selectivity in DSHP. Zhang *et al.*¹⁹ investigated the structure-activity relationship of different Pd nanocrystal (Pd(111) and Pd(100) facet) catalysts modified by a single Pt atom in DSHP (Fig. 4). They found that the PtPd(111) surface was more favorable for H_2O_2 formation due to its lower H_2 dissociation and O_2 two-step hydrogenation energy barrier compared to the PtPd(100). As a result, the obtained Pt_1Pd (111)/ TiO_2 catalyst showed outstanding catalytic performance, generating the highest H_2O_2 amount of $1921.3 \mu\text{mol}$ within 30 minutes, with an H_2 conversion of 62.2% and an H_2O_2 selectivity of 80.3%. Han *et al.*⁴⁰ found through DFT calculations that, compared to Pd(100) and Pd(110), the Pd(111) facet, with its higher coordination saturation and lower density of electronic states near the Fermi level, exhibited a higher activation energy barrier for the dissociation of O-O bonds, resulting in the highest reaction selectivity in the generation of H_2O_2 . The above works have deepened the researchers' understanding of the DSHP reaction mechanism.

Constructing Pd-M bimetal catalysts

In order to suppress the side reactions that are detrimental to H_2O_2 synthesis, researchers generally introduce a second metal to adjust the surface and interface microenvironment (*e.g.*, electronic structure, geometric structure, *etc.*) of Pd-based catalysts, aiming to enhance the efficiency of H_2O_2 synthesis. Au is the most commonly used second metal to enhance H_2O_2 productivity in DSHP.^{21,32,41-49} Hutchings *et al.*⁴¹ prepared a PdAu/carbon bimetallic alloy catalyst, in which the selectivity was increased from 34% to 80% and the productivity was doubled to $4.4 \text{ mol g}_{\text{Pd}}^{-1} \text{ h}^{-1}$ compared with that of the Pd/carbon catalyst. These results were mainly attributed to the ability of the nanoparticles to "turn off" the active sites on supports that promoted the decomposition and hydrogenation of H_2O_2 , thus improving the H_2O_2 selectivity. Additionally, Flaherty *et al.*⁴⁹ prepared PdAu nanoparticles with different ratios to adjust the coordination and isolation states of Pd. They found that increasing the isolation degree of Pd (*i.e.*, increasing the amount of Au) could enhance the H_2O_2 selectivity (Fig. 5), and an appropriate amount of Au could effectively improve the DSHP performance of Pd-based catalysts. They also proposed that the addition of Au atoms modified the electron distribution on the surface of Pd clusters, which in turn changed the activation energy of the radical reaction.⁴⁸ Xu *et al.*⁴² also achieved engineering control by adjusting the chemical state and geometric structure of the PdAu-PdAuO_x

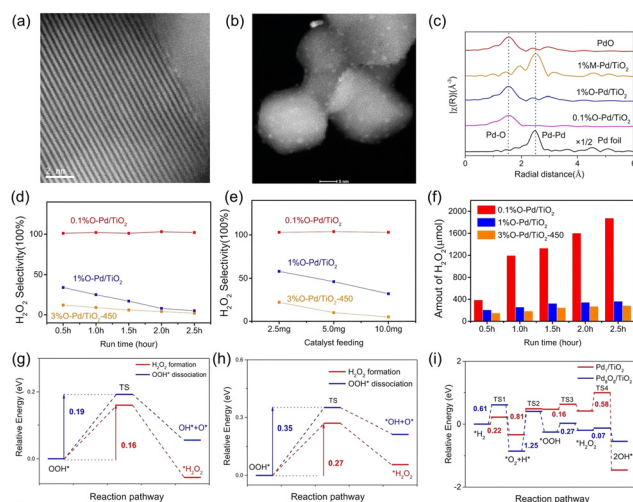


Fig. 3 HAADF-STEM images of (a) 0.1% O-Pd/ TiO_2 and (b) 1% O-Pd/ TiO_2 . (c) Fourier transforms of Pd K-edge EXAFS spectra for the catalysts, PdO, and Pd foil. H_2O_2 selectivity for (d) different reaction times and (e) different catalyst feedings. (f) Amounts of H_2O_2 for different reaction times. Reaction energy barriers for H_2O_2 formation and OOH dissociation on (g) Pd_1/TiO_2 and (h) $\text{Pd}_8\text{O}_8/\text{TiO}_2$. (i) The entire reaction potential energy landscape on Pd_1/TiO_2 and $\text{Pd}_8\text{O}_8/\text{TiO}_2$.³⁷

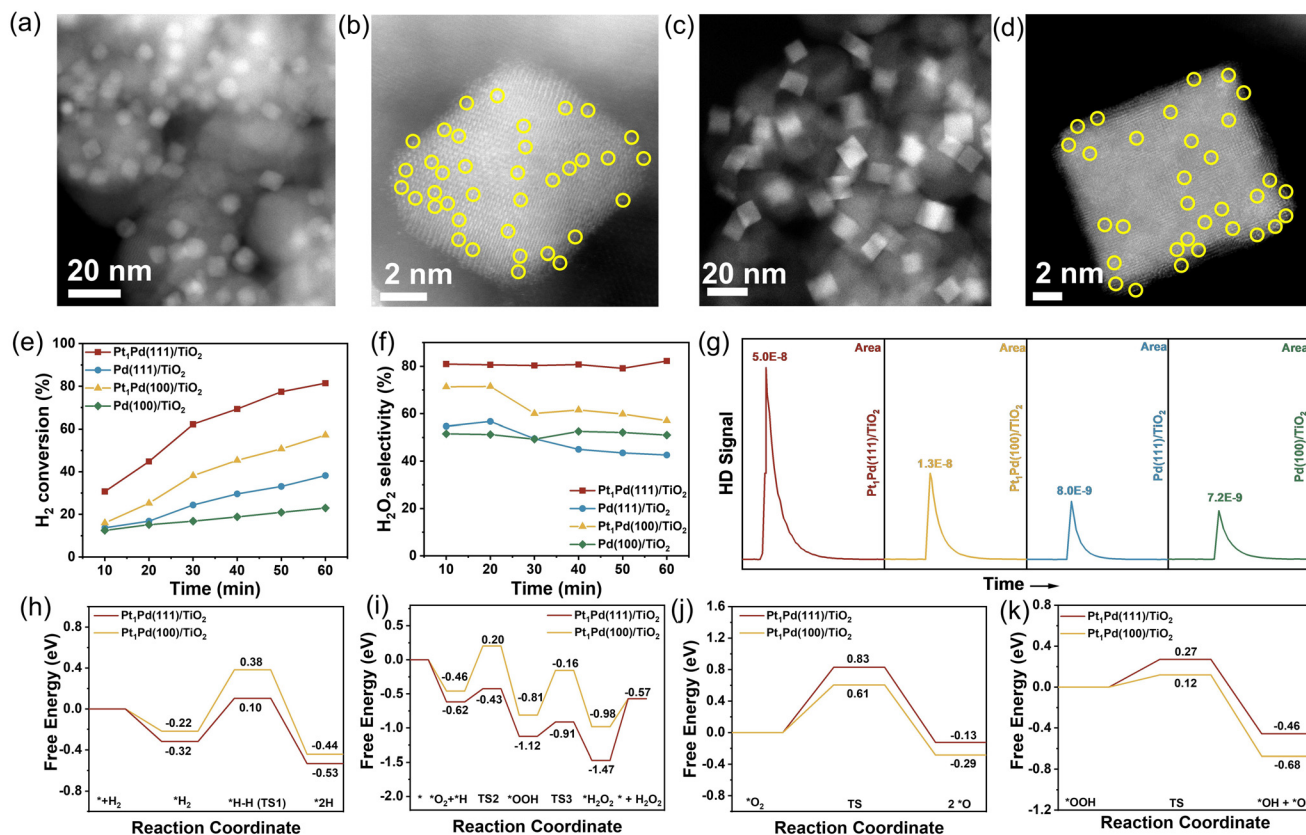


Fig. 4 The dark-field STEM image of the (a) PtPd(111) and (c) PtPd(100) nanocrystals supported on TiO₂. AC HAADF-STEM images of (b) PtPd(111)/TiO₂ and (d) PtPd(100)/TiO₂, single Pt atoms are highlighted by the yellow circles. Comparison of (e) H₂ conversion and (f) H₂O₂ selectivity as a function of H₂O₂ synthesis reaction time. (g) HD signal in H₂-D₂ exchange experiments at room temperature. Free energy profiles for (h) H₂ dissociation, (i) O₂ hydrogenation, (j) *O₂ dissociation, and (k) *OOH dissociation.¹⁹

interface, achieving a maximum selectivity of 87.7% for H₂O₂. Subsequently, Hutchings *et al.*^{50–52} employed similar PdAu catalysts (PdAu/TS-1) for the reaction of *in situ* generated H₂O₂ to efficiently produce oximes from ketones, achieving a selectivity of >95% for cyclohexanone oxime, comparable to current industrial routes. This process not only eliminates the need for transporting and storing highly concentrated, stable H₂O₂, but also contributes to being environmentally friendly and cost-effective. This DSHP process resulted in the formation of reactive oxygen species, including hydroxyl, hydrogen peroxide and superoxide radicals, that are more than 107 times stronger than equivalent amounts of premade H₂O₂ over an AuPd catalyst.¹⁶

Hutchings *et al.*⁵³ added Sn to Pd-based catalysts (Fig. 6), and through appropriate heat treatment cycles, they were able to shut down the sequential hydrogenation and decomposition reactions, achieving >95% selectivity for H₂O₂. This effect was attributed to the surface layer of tin oxide encapsulating small Pd-rich particles while allowing larger Pd–Sn alloy particles to remain exposed. Xiong *et al.*⁵⁴ developed a Pd–Sn nanowire catalyst (Pd_L/PdSn-NW) with a surface layer of PdO (Fig. 7). This catalyst showed a high H₂O₂ selectivity of >95% and an efficient productivity of 12.9 mol g_{Pd}⁻¹ h⁻¹, which was attrib-

uted to the different adsorption behaviors of O₂, H₂, and H₂O₂ on the Pd_L/PdSn-NW with bi-coordinated palladium. Furthermore, the weak adsorption of H₂O₂ on the Pd_L/PdSn-NW results in low activation energy and high H₂O₂ yield. To compare the roles of Au and Sn in Pd-based catalysts, Hutchings *et al.*⁵⁵ prepared a series of PdAu and PdSn catalysts by the wet co-impregnation method and compared their performance in the DSHP reaction. They found that considerable synergistic enhancement of catalytic performance could be obtained by introducing a relatively low loading of Au (Pd : Au = 1 : 1 (wt/wt)), but larger Sn loading was required to compete with the performance provided by the optimal PdAu ratio (Pd : Sn = 1 : 10 (wt/wt)).

Pt atoms have also been recognized as an effective metal capable of enhancing the DSHP performance on Pd-based catalysts. Zhang *et al.*⁵⁶ prepared fully exposed Pd cluster catalysts modified by trace Pt single atoms as electronic promoters by a simple impregnation method, which displayed an H₂O₂ productivity of 37.3 mol g_{Pd}⁻¹ h⁻¹ and 86.5% H₂O₂ selectivity in the DSHP reaction, remarkably superior to that of single metal fully exposed Pd cluster catalysts (Fig. 8). They found that the addition of trace Pt single atoms changed the electronic structures of Pd species, which significantly promoted the electron

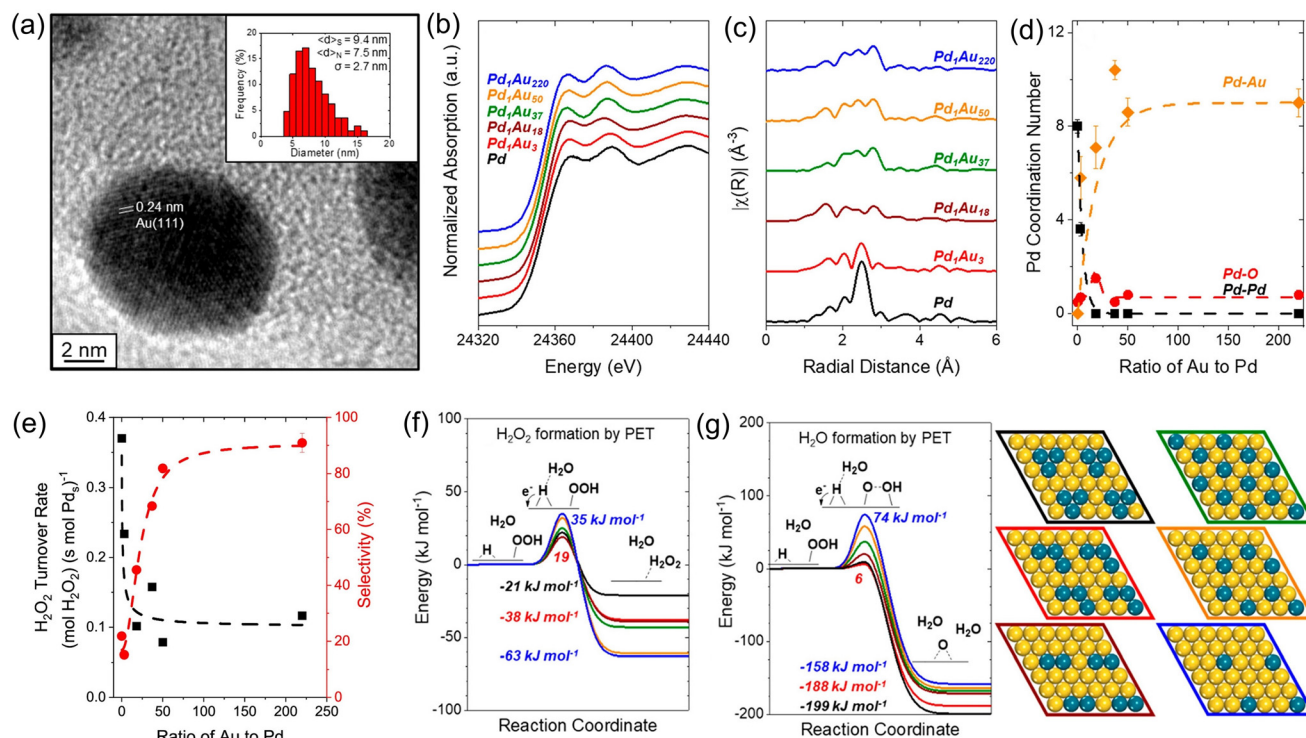


Fig. 5 (a) Representative TEM image of a Pd₁Au₅₀ nanoparticle showing lattice fringes consistent with Au(111). (b) XANES spectra and (c) EXAFS magnitudes of the Fourier-transformed k_2 -weighted Pd and Pd₁Au_x. (d) EXAFS best fit of Pd–Pd, Pd–Au, and Pd–O coordination numbers as a function of the atomic ratio of Au to Pd measured *in situ* (55 kPa H₂, 60 kPa O₂, 298 K). (e) Steady-state H₂O₂ turnover rates and primary H₂O₂ selectivity for Pd and Pd₁Au_x catalysts with a range of Au to Pd atomic ratios. DFT-calculated reaction coordinate diagrams for (f) H₂O₂ and (g) H₂O formation with the corresponding catalyst model.⁴⁹

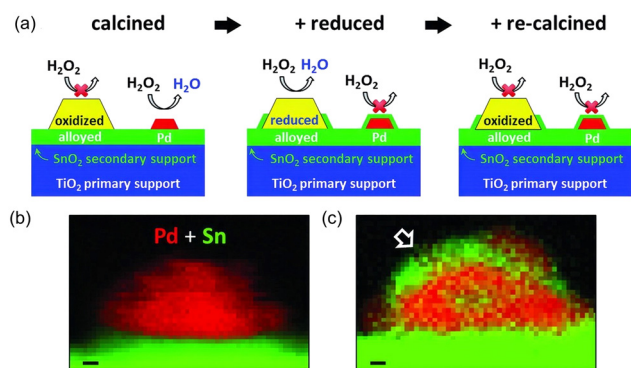


Fig. 6 Evolution of the catalyst through an oxidation–reduction–oxidation cycle. (a) Proposed mechanism for switching off H₂O₂ hydrogenation using small Pd-rich NPs through a strong metal–support interaction. STEM-EELS mapping of a 5 wt% Pd/SnO₂ model catalyst at the (b) oxidized and (c) O–R–O stages, showing partial encapsulation of the Pd NPs (red) by SnO_x (green) after the O–R–O heat treatment cycle. Scale bar, 1 nm.⁵³

transfer from Pt to Pd and then enhanced H₂ dissociation and inhibited O₂ dissociation, thereby promoting the generation of *OOH and ultimately obtaining a high productivity and selectivity of H₂O₂. Hutchings *et al.*^{29,30} also added a small amount of Pt (weight ratio 1 : 1) to the AuPd catalyst, which signifi-

cantly improved its DSHP performance. The synthesis and hydrogenation/decomposition processes were examined as independent datasets, and the activity values were superimposed as a fourth (vertical) dimension on the ternary composition diagram to establish the ideal ternary alloy composition for this reaction. Yu *et al.*^{57,58} also reported Pd@Pt core–shell nanocube catalysts with excellent H₂O₂ performance in DSHP.

In addition to Au, Sn, and Pt, which are commonly used to tailor the DSHP performance of Pd-based catalysts, Huang *et al.*⁵⁹ developed a Pd_xPb nanoring catalyst with a productivity of 5.7 mol g_{Pd}^{−1} h^{−1}. The addition of Pb (especially at the edge and corner preferential positions) can significantly reduce the number of low-coordination Pd atoms. This unique structure facilitated the formation of the key intermediate *OOH and inhibited the dissociation of O₂ to form H₂O, thereby increasing the productivity and selectivity of H₂O₂ while reducing the degradation rate. At the same time, Behrens *et al.*⁶⁰ reported an intermetallic Pd₃Pb nanocrystal catalyst and compared the DSHP catalytic performances of cubic, cuboctahedral, and spherical-shaped Pd₃Pb nanocrystals. They found that the catalytic efficiency of DSHP was influenced not only by the nanocrystal composition, but also by the particle shape. The catalytic performance of Pd₃Pb cubes (with major terminations on the (200) facet) was superior not only to monometallic Pd catalysts, but also to Pd₃Pb nanocrystals with other shapes.

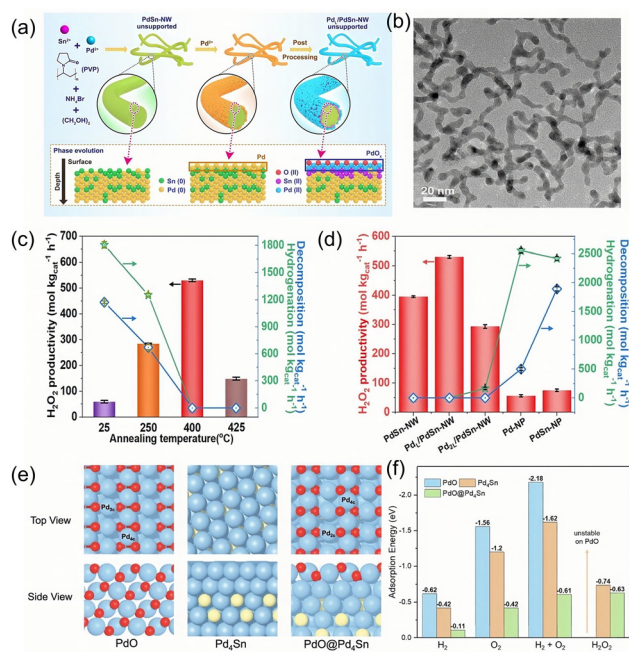


Fig. 7 (a) Schematic illustration of the synthesis of unsupported PdSn-NW and Pd_L/PdSn-NW. (b) A representative TEM image of the unsupported PdSn nanowire catalyst prepared by a two-step method (unsupported Pd_L/PdSn-NW). H₂O₂ productivity, hydrogenation, and decomposition of (c) the supported PdL/PdSn-NW catalyst annealed at different temperatures in air and (d) supported Pd_L/PdSn-NW catalyst with other Pd catalysts. (e) DFT optimized structures of PdO(101), Pd₄Sn, and PdO@Pd₄Sn with (f) adsorption energies of H₂, O₂, H₂ + O₂, and H₂O₂.⁵⁴

Additionally, Ag,⁶¹ Te,^{62,63} Sb,⁶⁴ Ga,⁶⁵ In,⁶⁵ W,^{66,67} Fe,⁶⁸ Co,^{69,70} Ni,^{71–74} Zn,⁷⁵ etc. were also employed as second metal promoters to enhance the DSHP performance.

From the above results, it is evident that constructing Pd–M bimetal catalysts is a common and effective method to enhance the performance of DSHP. Compared to the catalytic activity of monometallic Pd catalysts, the selectivity and productivity of Pd–M bimetal catalysts tend to be significantly better, which is instructive for the development of Pd–M bimetal catalysts for DSHP.

Confinement structure

Encapsulating active sites in a confinement structure can adjust atomic arrangement, electronic transfer, and coordination while decoupling mass transfer from the reaction and enhancing effective collisions between molecules or atoms. Rational utilization of these properties for the preparation and modulation of catalysts is an effective way to improve the performance of DSHP.^{76,77} Wang *et al.*⁷⁸ demonstrated that by encapsulating small Pd nanoparticles encapsulated in Sn-containing MFI zeolite crystals (Pd–SnO_x@MFI, Fig. 9), where Sn acts as an electron donor, they can effectively reduce the adsorption of molecular O₂ and inhibit O–O bond cleavage, thereby preventing Pd oxidation. This structurally stable Pd–SnO_x@MFI catalyst exhibited exceptional performance in

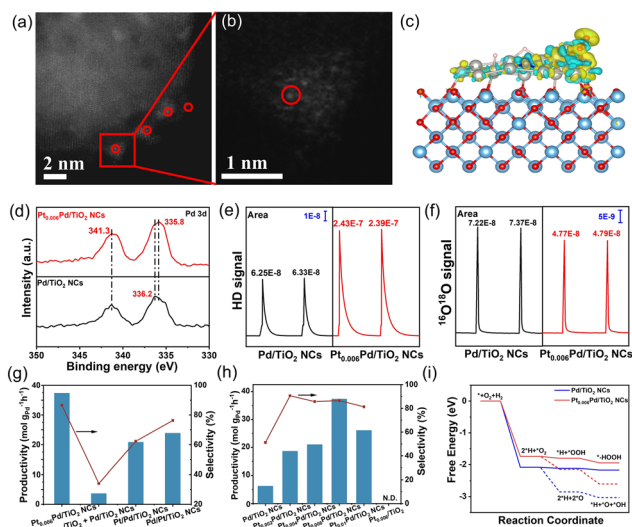


Fig. 8 AC HAADF-STEM images of Pt_{0.006}Pd/TiO₂ NCs at (a) low and (b) high magnifications, single-atom Pt sites are highlighted by the red circles. Differential charge density of O₂ adsorption on (c) Pt_{0.006}Pd/TiO₂ NC surface (the yellow and cyan colors represent the increase and decrease of charge density, respectively). (d) Pd 3d XPS spectra, (e) the HD signal in H₂–D₂ exchange experiments, and (f) ¹⁶O¹⁸O signal in ¹⁶O₂–¹⁸O₂ exchange experiments for Pt_{0.006}Pd/TiO₂ NCs and Pd/TiO₂ NCs. H₂O₂ productivity and selectivity on catalysts of (g) one-step and two-step impregnation and (h) different Pt contents in the direct synthesis of H₂O₂. (i) Energy profiles for H₂O₂ synthesis on Pt_{0.006}Pd/TiO₂ NC and Pd/TiO₂ NC surfaces.⁵⁶

DSHP, achieving a H₂O₂ productivity of 10.2 mol g_{Pd}^{−1} h^{−1}, which surpassed the performance of previously reported catalysts. They also prepared aluminosilicate zeolite-encapsulated PdAu nanoparticle catalysts with an H₂O₂ productivity of 0.32 mol g_{PdAu}^{−1} h^{−1} and a selectivity of 88% in pure water.⁷⁹ This unique structure can assist proton transfer and catalyze oxygen hydrogenation to generate H₂O₂. Huang *et al.*⁸⁰ developed a Pd-based catalyst with a Pd core and an NiO shell (Pd@NiO). The NiO shell not only provided a reaction channel for H₂ and O₂ to contact the Pd active sites, but also significantly reduced the strong bonding between Pd and the intermediate (O–O)* due to its modifying effect on the Pd core. This Pd@NiO catalyst ultimately achieved a high H₂O₂ selectivity of 91% along with excellent stability. Similarly, Pan *et al.*⁸¹ synthesized a yolk–shell nanocatalyst, Pd@HCS, which demonstrated a productivity of 3.2 mol g_{Pd}^{−1} h^{−1} and a selectivity of 94% in the DSHP reaction. This confinement structure is also effective for the oxidation reaction using *in situ* produced H₂O₂. Yamashita *et al.*⁸² developed a core–shell structured Pd/SiO₂@Ti-MS catalyst consisting of Pd nanoparticles (NPs) loaded on SiO₂ cores covering a Ti-containing mesoporous silica (Ti-MS) shell layer. The efficiency of *in situ* generated H₂O₂ could be significantly enhanced by modulating the Pd NP position, pore size and the thickness of the Ti-MS shell layer. Compared with the supported Pd/TS-1 catalyst, the activity of Pd/SiO₂@Ti-MS for the oxidation of methyl phenyl sulfide was enhanced by 20 times.

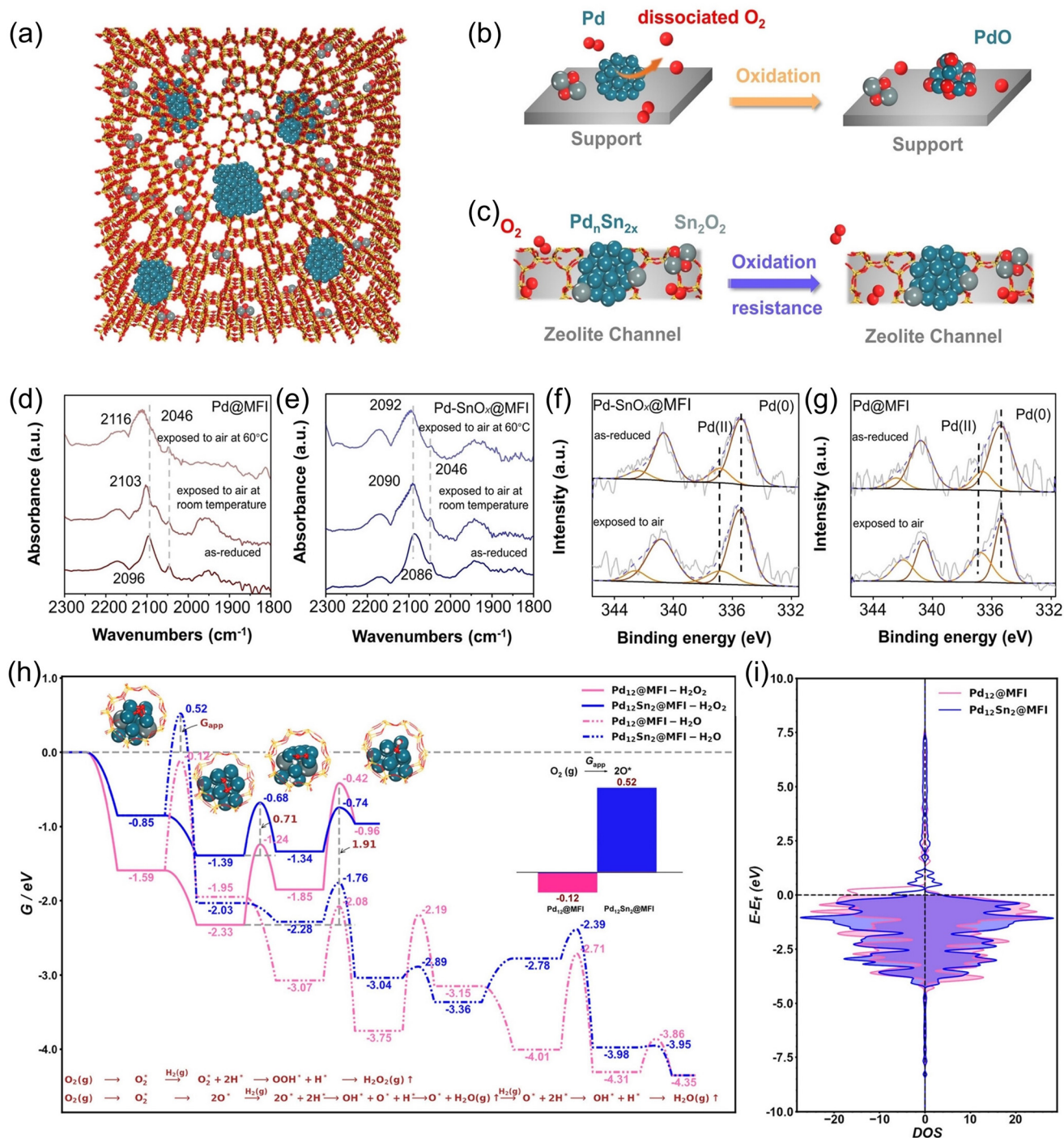


Fig. 9 Scheme showing (a) the structure of Pd-SnO_x@MFI. Oxidation of Pd and oxidation resistance of PdSn by providing (b) dissociation and (c) hindered dissociation of the O-O bond. CO-adsorption DRIFTS of (d) Pd@MFI and (e) Pd-SnO_x@MFI samples. Pd 3d XPS spectra of (f) Pd-SnO_x@MFI and (g) Pd@MFI samples. (h) Apparent free energy barriers (G_{app}) of O₂ activation, Gibbs free energy profiles of H₂O₂ synthesis, and water formation over Pd₁₂Sn₂@MFI and Pd₁₂@MFI (the corresponding intermediate of each elementary step is shown in brown under the energy profile) at 25 °C. (i) Projected density of states of the spin-polarized Pd d orbitals of Pd₁₂@MFI and Pd₁₂Sn₂@MFI.⁷⁸

Ligand modification

Surface ligand modification of the active sites in catalysts can provide stable nanostructures and morphologies while also significantly influencing active site selection, steric hin-

drance, and interfacial electronic effects.⁸³ Ramírez *et al.*⁸⁴ developed a carbon-supported hexadecyl-2-hydroxyethyl-dimethyl ammonium dihydrogen phosphate (C₂₀H₄₆NO₅P)-capped Pd nanoparticle catalyst (Fig. 10a-c). The experimental results indicated that as the ligand content

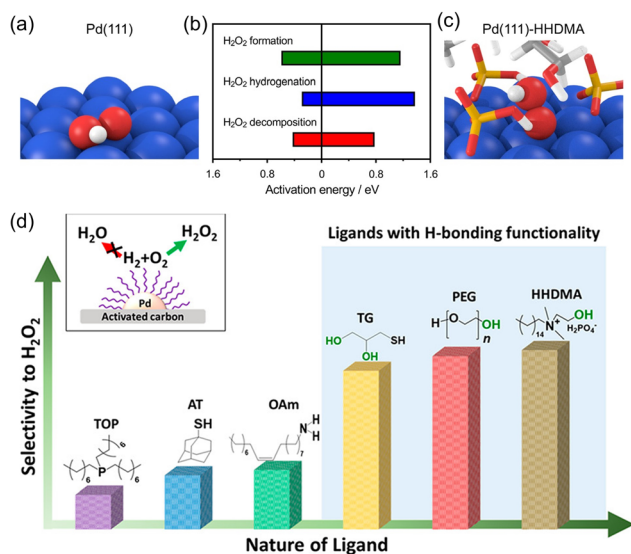


Fig. 10 The adsorption configuration of the hydroperoxy (OOH) radical on (a) Pd(111)- and (c) Pd(111)-HHDMA surfaces. Color code: H in white, C in grey, O in red, P in yellow, and Pd in blue. (b) Activation energies for the direct synthesis of H₂O₂ and the side reactions leading to water formation by H₂O₂ hydrogenation and decomposition.⁸⁴ (d) The H₂O₂ selectivity of catalysts with various ligands.⁸⁵

increased, the selectivity for H₂O₂ also increased, reaching 80%, with the corresponding H₂O₂ productivity achieving 8.4 mol g_{Pd}⁻¹ h⁻¹. This behavior was attributed to the unique vertical adsorption mode caused by the electrostatic interactions between the reaction intermediates and the ligands, which prevented further dissociation and hydrogenation of H₂O₂. Subsequently, they further investigated the effects of different ligand modifications (including phosphines, thiols, and weakly bound molecules) on DSHP performance and found that catalysts with hydrogen-bonding group ligands achieved the optimal H₂O₂ synthesis performance (Fig. 10d).⁸⁵ Hutchings *et al.*⁸⁶ reported a Pd-based catalyst modified with N-heterocyclic carbenes (NHCs), which displayed significantly improved catalytic performance compared to unmodified Pd-based catalysts. The enhanced performance was attributed to the electronic modification of the Pd species by the NHCs. Recently, Chen *et al.*⁸⁷ reported an amino-functionalized Pd-based catalyst supported on SBA-15 with strong metal-support interactions. The amino modification increased the proportion of Pd⁰, facilitating the adsorption and conversion of H₂ and O₂. Additionally, they found that the hydrogen bonding interactions between the amino groups and H₂O₂ effectively suppressed the hydrogenation and decomposition of H₂O₂, ultimately improving H₂O₂ selectivity and productivity. Ligand modification is an effective strategy to enhance DSHP performance, but it can also increase the complexity and cost of catalyst preparation. In addition, some ligands may also be susceptible to desorption during the DSHP reaction, leading to reduced reusability of the catalyst.

Microenvironment modulation strategies on supports

Supports are critical in catalytic reactions, as their surface properties profoundly influence the catalytic activity, selectivity, and stability. In the DSHP reaction, supports in Pd-based catalysts have predominantly focused on oxides, carbon materials, molecular sieves, and heteropoly acids. Researchers have leveraged the inherent properties of these supports to further optimize their structures, thereby enhancing the interaction between the support and the active sites. This optimization aims to develop more effective supports that improve the efficiency of H₂O₂ production.

Acid regulation

In the DSHP reaction, the acidic system is more conducive to the generation of H₂O₂. However, the addition of inorganic acids poses problems such as corrosion of reaction equipment and difficulties in separation. In recent years, researchers have focused on adjusting the acidity of the support surface to enhance the efficiency of H₂O₂ production.^{88–90} Cheng *et al.*⁹¹ prepared a series of PdAu nanoparticle catalysts supported on SiO₂-modified Al₂O₃. They adjusted the number of Brønsted acid sites by varying the SiO₂ content on the Al₂O₃ surface. They found that the increase in Brønsted acid sites can accelerate the H₂ conversion to H. The adsorbed H dissociated from H₂ at the Brønsted acid sites will spillover to the PdAu nanoparticles through the support, creating a new reaction pathway for the hydrogenation of adsorbed O₂ to produce H₂O₂. But this method also enhances the ability of H₂O₂ hydrogenation. Hutchings *et al.*^{92–94} adjusted the surface acidity of the catalyst by performing acid pretreatment on the support. They found that the acid pretreatment of the support can enhance the dispersion of Au in the catalyst, leading to an increased proportion of smaller PdAu nanoparticles. This variation in particle size distribution is the key to enhance the activity of the catalyst. Furthermore, they also investigated the use of Cs-exchanged phosphotungstic acid (Cs_xH_{3–x}PW₁₂O₄₀) as a support for Pd-based catalysts and achieved higher H₂O₂ productivity.⁹⁵ Acidic regulation plays a role in enhancing the reactivity of the DSHP reaction. However, if the acidity is too strong, it may lead to the leaching of active metals, which can negatively impact the performance of the DSHP reaction.

Heteroatom doping

Heteroatom (B,⁹⁶ C,⁹⁷ N,⁹⁸ P,⁹⁹ S,¹⁰⁰ Br¹⁰¹) doping is also commonly used to adjust the structural properties of supports to enhance the catalytic activity in DSHP. Ouyang *et al.*⁹⁶ developed a catalyst (Pd/B-TiO₂) by doping boron (B) atoms at the interface between Pd and TiO₂ (Fig. 11a–d). Compared to the undoped catalyst (Pd/TiO₂), Pd/B-TiO₂ exhibited an increase in H₂O₂ selectivity and productivity, increasing from 63.4% and 2.99 mol g_{Pd}⁻¹ h⁻¹ to 80.1% and 3.65 mol g_{Pd}⁻¹ h⁻¹, respectively. They found that B doping can strengthen the interaction between Pd nanoparticles and TiO₂, which altered

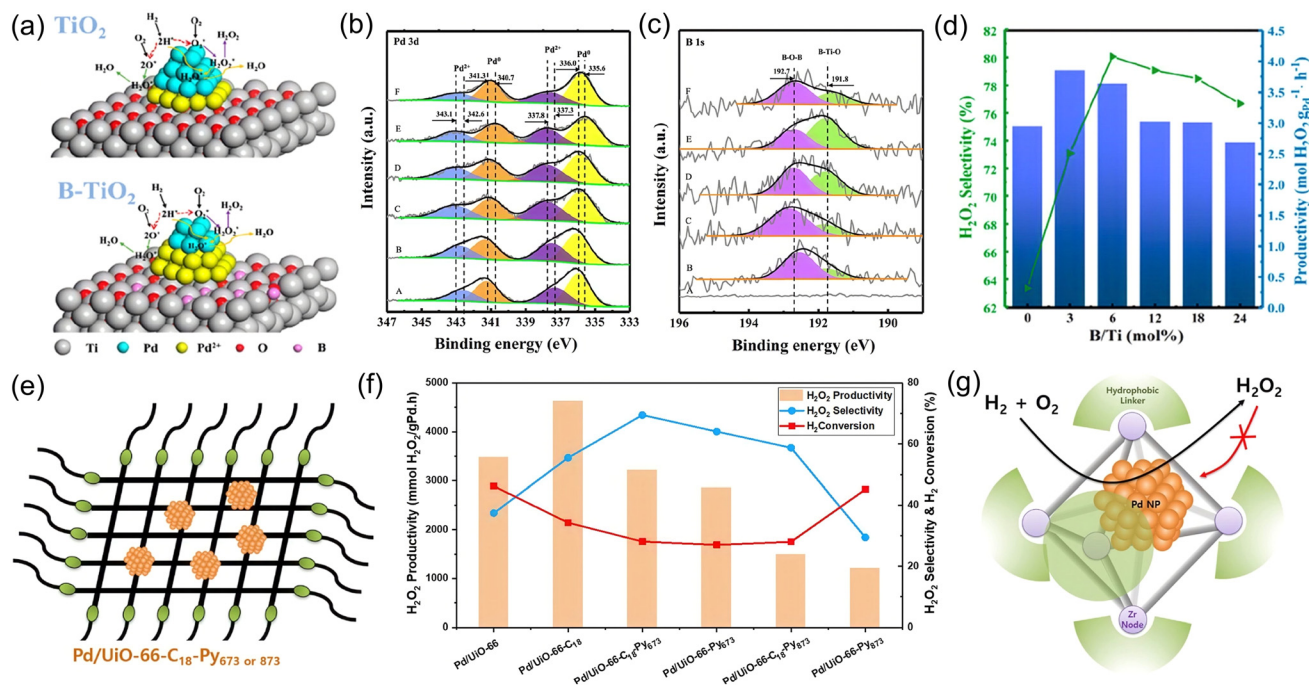


Fig. 11 (a) The scheme of H₂O₂ formation on Pd/TiO₂ and Pd/B-TiO₂. High-resolution (b) Pd 3d and (c) B 1s XPS spectra of catalysts with different boron amounts: (A) 1% Pd/TiO₂, (B) 1% Pd/B-TiO₂ (3%), (C) 1% Pd/B-TiO₂ (6%), (D) 1% Pd/B-TiO₂ (12%), (E) 1% Pd/B-TiO₂ (18%), and (F) 1% Pd/B-TiO₂ (24%). (d) The H₂O₂ selectivity and productivity on Pd/B-TiO₂ catalysts with different B/Ti ratios.⁹⁶ (e) The scheme of Pd/Uio-66-C₁₈-Py₆₇₃ or 873. (f) Effect of incorporation of the hydrophobic linker and subsequent pyrolysis on the reaction performance of the Pd/Uio-66 catalyst for direct synthesis of H₂O₂. (g) Illustration of the prevention of H₂O₂ from reapproaching active sites, which are surrounded by hydrophobic linker molecules.¹⁰²

the surface atomic configuration, thus increasing the proportion of Pd²⁺ and providing more active sites for the non-dissociative activation of O₂. Additionally, the electronic effects between B and Pd also facilitated the adsorption and activation of H₂, thereby improving both the selectivity and productivity of H₂O₂. Liu *et al.*⁹⁷ enhanced the hydrophobicity of TiO₂-supported catalysts by doping with carbon (C). This doping reduced the adsorption energy of H₂O₂, thereby accelerating H₂O₂ desorption. Additionally, the C doping also stabilized the interaction between Pd nanoparticles and TiO₂. Sulfur (S) was also an excellent dopant for enhancing the interaction between active sites and the support. Zhu *et al.*¹⁰⁰ developed an S-doped carbon-supported Pd catalyst. The S doping not only facilitated the dispersion of Pd nanoparticles, but also enhanced the adsorption of H₂ on the catalyst surface. As a result, the H₂O₂ productivity was 4.8 times higher compared to the undoped catalyst. Heteroatom doping is an effective strategy for catalyst modification, but the effect of doping on the structural stability of the catalyst should also be concerned during design and preparation in order to prevent deactivation during catalysis.

Surface functionalization

Modifying the surface of the catalyst support to introduce specific functional groups and alter the chemical properties of the support is also a method to regulate the microenvironment

of the catalyst, which can significantly affect the performance of the DSHP reaction. Chung *et al.*¹⁰² functionalized the outer surface of UiO-66 by incorporating C₁₈ hydrophobic linkers onto the Zr metal nodes to increase the hydrophobicity of the Pd/Uio-66 catalyst (Fig. 11e–g). They found that the presence of C₁₈ hydrophobic groups effectively prevented the adsorption of H₂O₂, thereby enhancing the selectivity for H₂O₂. Further pyrolysis of the resulting Pd/Uio-66-C₁₈ catalyst could lead to an additional increase in selectivity. However, this increase in selectivity came at the expense of reduced H₂ conversion due to an increase in mass transfer resistance. Chen *et al.*¹⁰³ used oxygen- and nitrogen-functionalized mesoporous carbon as the support to prepare the Pd/OMC catalyst. The nitrogen functional groups can effectively regulate the ratio of Pd²⁺, thereby achieving high H₂O₂ selectivity. Hutchings *et al.*¹⁰⁴ introduced acidic oxygen functional groups onto the surface of carbon nanofibers to suppress the undesirable side reactions in the DSHP reaction. This method has also been applied to the oxidation of CH₄ using *in situ* generated H₂O₂. Xiao *et al.*¹⁰⁵ combined a surface functionalization strategy with a confinement structure strategy to prepare PdAu@ZSM-5-C₁₆ molecular-fence catalysts by anchoring AuPd alloy nanoparticles in aluminosilicate zeolite crystals and then modifying the external surface of the zeolite with organosilanes (Fig. 12). The modified surface of the zeolite allows the diffusion of H₂, O₂ and CH₄ into the active sites, while confining the generated H₂O₂ in the catalyst,

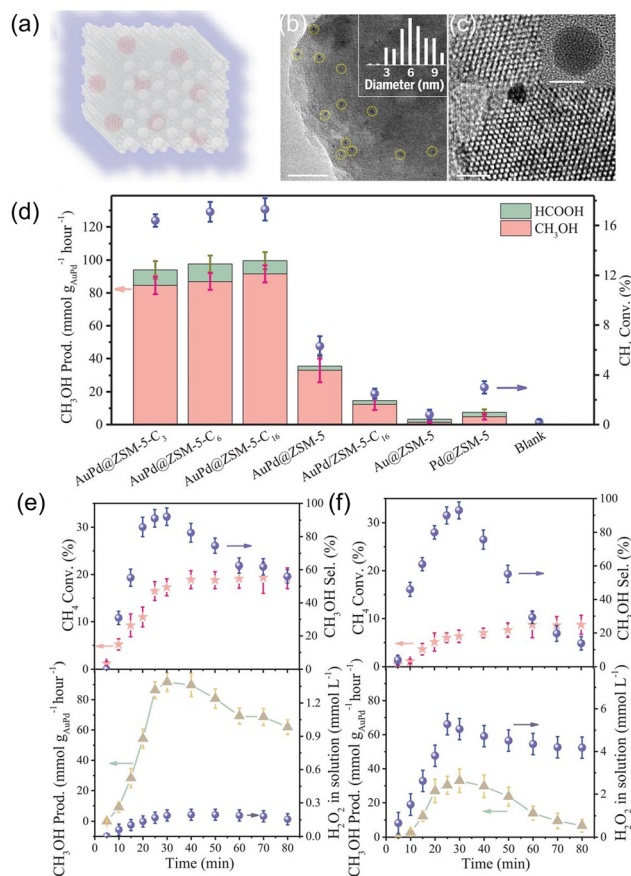


Fig. 12 Models and tomographic section TEM images of (a–c) AuPd@ZSM-5-C₁₆. (d) Data characterizing the oxidation of methane with H₂ and O₂ over various catalysts. Dependences of methane conversion (Conv.), methanol selectivity (Sel.), methanol productivity (Prod.), and H₂O₂ concentration in water solution on reaction time over (e) AuPd@ZSM-5-C₁₆ and (f) AuPd@ZSM-5 catalysts.¹⁰⁵

thus increasing the local H₂O₂ concentration and CH₄ oxidation efficiency, the corresponding CH₄ conversion reached 17.3% with 92% selectivity of CH₃OH.

Table 1 compares the performance of palladium-based catalysts with microenvironment regulation strategies for DSHP in recent years. Optimizing the local properties of the catalyst interface can significantly enhance the activity in specific reactions, particularly in improving the selectivity for H₂O₂.

Conclusions and perspectives

The DSHP reaction has attracted significant attention due to its green, efficient, and economical manufacturing process. In recent years, researchers have made notable progress in developing DSHP-Pd-based catalysts. A series of approaches to modulate the microenvironment of catalysts were developed, such as adjusting the valence and morphology of active sites, constructing bimetallic Pd–M catalysts, creating confined structures, introducing functional groups, modulating acidity, doping heteroatoms, *etc.*, to optimize the catalyst surface–interface structure, which ultimately achieved the purpose of suppressing the side reactions and improving the H₂O₂ selectivity and productivity. These advancements also provide valuable guidance for the design of high-efficiency DSHP catalysts in the future.

However, there are still many issues that need to be addressed in DSHP research on the road to industrialization. Firstly, to ensure the safe conduct of the DSHP reactions, most works (especially those using batch reactors) control the H₂ content at very low levels to avoid explosion risks. However, at such low H₂ content, the resulting H₂O₂ concentration is too low, requiring repeated separation and concentration processes, which will increase the production costs. Microreactors are a reliable choice for avoiding H₂ explosion in DSHP. Due to its large specific surface area and rapid mass and heat transfer, H₂ and O₂ can mix and react quickly, and the heat generated can be rapidly removed, making it difficult for flames to propagate. Consequently, the concentrations of H₂ and O₂ in microreactors are no longer limited by explosion thresholds, providing the potential for achieving high H₂O₂ concentrations

Table 1 The comparison of the DSHP performances on Pd-based catalysts

Catalysts	Solvents	Promoters	Reaction conditions	Conversion (%)	Selectivity (%)	Productivity (mol g _{Pd} ⁻¹ h ⁻¹)	Ref.
Pt ₁ Pd(111)/TiO ₂	MeOH	HCl	0 °C, 4 MPa, 30 min	62.2	80.3	11.8	19
Pd/SiO ₂	H ₂ O	NaBr	20 °C, 0.1 MPa	—	36	10.8	27
0.5% Au–0.5% Pd/TiO ₂	MeOH/H ₂ O	CO ₂	2 °C, 4 MPa, 30 min	24.4	53.1	19.2	31
2.5% Au/2.5% Pd/carbon	MeOH/H ₂ O	CO ₂	2 °C, 4 MPa, 30 min	—	80.0	4.4	41
3 wt% Pd–2 wt% Sn/TiO ₂	MeOH/H ₂ O	CO ₂	2 °C, 4 MPa, 30 min	9.0	96.0	2.0	53
Pd ₁ /PdSn–NW	MeOH/H ₂ O	—	2 °C, 4 MPa, 15 min	22.1	95.3	12.8	54
Pt _{0.006} Pd/TiO ₂ NCS	MeOH	HCl	0 °C, 4 MPa, 30 min	40.1	86.5	37.3	56
Pd ₆ Pb NRs/TiO ₂ –H–A	MeOH/H ₂ O	—	0 °C, 4 MPa, 30 min	39.1	56.7	5.7	59
1% Pd–5% Zn/Al ₂ O ₃	MeOH	H ₂ SO ₄	2 °C, 3 MPa, 15 min	56.6	78.5	25.4	75
PdAu@HZSM-5	H ₂ O	—	2 °C, 4 MPa, 30 min	15.3	88	0.63	79
Pd@NiO-3/TiO ₂	MeOH/H ₂ O	—	2 °C, 4 MPa, 15 min	—	91.0	1.8	80
Pd–HDDMA/C	MeOH/H ₂ O	—	0 °C, 4 MPa, 30 min	9.7	79.8	12.8	85
Pd/SBA-15-3–NH ₂ –3	MeOH	H ₂ SO ₄	0 °C, 0.1 MPa	18.2	94.5	6.2	87
Pd/B–TiO ₂	EtOH	H ₂ SO ₄	10 °C, 0.1 MPa	12.2	80.1	3.7	96
Pd/UiO-66–C ₁₈ Py ₆₇₃	MeOH/H ₂ O	—	2 °C, 3 MPa, 60 min	—	70.0	3.2	102

of DSHP reactions in the future. Furthermore, membrane catalysts that segregate hydrogen from oxygen are also a popular alternative. Secondly, the optimization of the reaction process is also an important research direction. The DSHP process needs to be carried out at specific temperature and pressure, also with low utilization of H₂, so fine-tuning the reaction conditions, deeply elucidating the reaction mechanism, and establishing a reaction kinetic model will help to improve the productivity and selectivity of H₂O₂ relying on artificial intelligence and big data analytics. Thirdly, there is a need for optimization and innovation in catalysts. The resulting H₂O₂ concentration is still very low owing to the inefficient catalysts, and it is not yet economically viable to replace the anthraquinone method. More efficient and stable catalysts should be explored in the future, such as by developing new types of non-Pd or non-noble-based catalysts, as well as by adjusting the microenvironment of catalysts to improve the catalytic efficiency and selectivity. Additionally, incorporating the latest technology in nanocatalysis and characterization is also a promising way to develop new DSHP catalysts with superior performance. Finally, the scale-up and economics of catalyst production are huge issues. Although significant progress has been made in laboratory research, it is still a challenge to maintain the performance of the catalyst and reduce the production cost in large-scale production.

In summary, the DSHP process is a green production technique with broad application prospects. Currently, it is more suitable for producing small amounts of low-concentration H₂O₂, such as in on-site applications in the medical and electronics industries, where “ready-to-use” production is required. We believe that with continuous optimization in catalyst technology, reaction processes, and production costs, this process will play a significant role in areas such as environmental protection, energy conversion, and chemical production.

Author contributions

The manuscript was written through the contributions of all authors. Xiaohui He and Ying Zhang developed the concept. Ying Zhang, Xilun Wang, Ziyue Wang, and Liyang Liu wrote the paper. Xiaohui He and Hongbing Ji directed the project.

Data availability

The data supporting this article have been included within the text.

Conflicts of interest

There are no conflicts to declare.

Acknowledgements

This work was supported by the National Key Research and Development Program Nanotechnology Specific Project (No. 2020YFA0210900), the Guangdong Natural Science Funds for Distinguished Young Scholar (2022B1515020035), the National Natural Science Foundation of China (22078371, U22A20428, 21961160741, 22422815), and the Special Fund for Science and Technology Innovation Teams of Shanxi Province (202304051001007). The authors thank the Guangdong Basic Research Center of Excellence for Functional Molecular Engineering and the Chemistry and Chemical Engineering Guangdong Laboratory (Grant No. 1922010).

References

- 1 J. M. Campos-Martin, G. Blanco-Brieva and J. L. G. Fierro, *Angew. Chem., Int. Ed.*, 2006, **45**, 6962–6984.
- 2 K. Dong, Y. Lei, H. Zhao, J. Liang, P. Ding, Q. Liu, Z. Xu, S. Lu, Q. Li and X. Sun, *J. Mater. Chem. A*, 2020, **8**, 23123–23141.
- 3 G. Gao, Y. Tian, X. Gong, Z. Pan, K. Yang and B. Zong, *Chin. J. Catal.*, 2020, **41**, 1039–1047.
- 4 G. H. Han, S. H. Lee, S. Y. Hwang and K. Y. Lee, *Adv. Energy Mater.*, 2021, **11**, 2003121.
- 5 L. Wang, J. Zhang, Y. Zhang, H. Yu, Y. Qu and J. Yu, *Small*, 2022, **18**, e2104561.
- 6 S. Ranganathan and V. Sieber, *Catalysts*, 2018, **8**, 379.
- 7 Y. Yi, L. Wang, G. Li and H. Guo, *Catal. Sci. Technol.*, 2016, **6**, 1593–1610.
- 8 Y. Guo, X. Tong and N. Yang, *Nano-Micro Lett.*, 2023, **15**, 77.
- 9 Y. Guo, C. Dai, Z. Lei, B. Chen and X. Fang, *Catal. Today*, 2016, **276**, 36–45.
- 10 A. G. Fink, R. S. Delima, A. R. Rousseau, C. Hunt, N. E. LeSage, A. Huang, M. Stolar and C. P. Berlinguette, *Nat. Commun.*, 2024, **15**, 766.
- 11 A. A. Ingle, S. Z. Ansari, D. Z. Shende, K. L. Wasewar and A. B. Pandit, *Environ. Sci. Pollut. Res. Int.*, 2022, **29**, 86469–86484.
- 12 H. Song, L. Wei, L. Chen, H. Zhang and J. Su, *Top. Catal.*, 2020, **63**, 895–912.
- 13 S. Siahrostami, S. J. Villegas, A. H. Bagherzadeh Mostaghimi, S. Back, A. B. Farimani, H. Wang, K. A. Persson and J. Montoya, *ACS Catal.*, 2020, **10**, 7495–7511.
- 14 M. Kou, Y. Wang, Y. Xu, L. Ye, Y. Huang, B. Jia, H. Li, J. Ren, Y. Deng, J. Chen, Y. Zhou, K. Lei, L. Wang, W. Liu, H. Huang and T. Ma, *Angew. Chem., Int. Ed.*, 2022, **61**, e202200413.
- 15 J. Liu, Z. Gong, M. Yan, G. He, H. Gong, G. Ye and H. Fei, *Small*, 2021, **18**, e2103824.
- 16 T. Richards, J. H. Harrhy, R. J. Lewis, A. G. R. Howe, G. M. Suldecki, A. Folli, D. J. Morgan, T. E. Davies, E. J. Loveridge, D. A. Crole, J. K. Edwards, P. Gaskin, C. J. Kiely, Q. He, D. M. Murphy, J.-Y. Maillard, S. J. Freakley and G. J. Hutchings, *Nat. Catal.*, 2021, **4**, 575–585.
- 17 G. J. Hutchings, *J. Catal.*, 2024, **432**, 115392.

- 18 M. Selinsek, B. J. Deschner, D. E. Doronkin, T. L. Sheppard, J.-D. Grunwaldt and R. Dittmeyer, *ACS Catal.*, 2018, **8**, 2546–2557.
- 19 Y. Zhang, Q. D. Sun, Z. Y. Wang, G. H. Guo, H. Liu, X. H. He and H. B. Ji, *Chem. Sci.*, 2024, **15**, 9830–9841.
- 20 R. J. Lewis and G. J. Hutchings, *ChemCatChem*, 2019, **11**, 298–308.
- 21 H. Xu, D. Cheng and Y. Gao, *ACS Catal.*, 2017, **7**, 2164–2170.
- 22 P. Tian, D. Ding, Y. Sun, F. Xuan, X. Xu, J. Xu and Y.-F. Han, *J. Catal.*, 2019, **369**, 95–104.
- 23 Z. Yao, J. Zhao, R. J. Bunting, C. Zhao, P. Hu and J. Wang, *ACS Catal.*, 2021, **11**, 1202–1221.
- 24 N. Agarwal, L. Thomas, A. Nasrallah, M. A. Sainna, S. J. Freakley, J. K. Edwards, C. R. A. Catlow, G. J. Hutchings, S. H. Taylor and D. J. Willock, *Catal. Today*, 2021, **381**, 76–85.
- 25 A. Akram, G. Shaw, R. J. Lewis, M. Piccinini, D. J. Morgan, T. E. Davies, S. J. Freakley, J. K. Edwards, J. A. Moulijn and G. J. Hutchings, *Catal. Sci. Technol.*, 2020, **10**, 8203–8212.
- 26 Y. Han and J. Lunsford, *J. Catal.*, 2005, **230**, 313–316.
- 27 P. Priyadarshini, T. Ricciardulli, J. S. Adams, Y. S. Yun and D. W. Flaherty, *J. Catal.*, 2021, **399**, 24–40.
- 28 V. Choudhary and C. Samanta, *J. Catal.*, 2006, **238**, 28–38.
- 29 J. K. Edwards, J. Pritchard, L. Lu, M. Piccinini, G. Shaw, A. F. Carley, D. J. Morgan, C. J. Kiely and G. J. Hutchings, *Angew. Chem., Int. Ed.*, 2014, **53**, 2381–2384.
- 30 J. K. Edwards, J. Pritchard, P. J. Miedziak, M. Piccinini, A. F. Carley, Q. He, C. J. Kiely and G. J. Hutchings, *Catal. Sci. Technol.*, 2014, **4**, 3244–3250.
- 31 J. Brehm, R. J. Lewis, D. J. Morgan, T. E. Davies and G. J. Hutchings, *Catal. Lett.*, 2022, **152**, 254–262.
- 32 J. K. Edwards, A. Thomas, A. F. Carley, A. A. Herzing, C. J. Kiely and G. J. Hutchings, *Green Chem.*, 2008, **10**, 388–394.
- 33 V. Paunovic, V. V. Ordonsky, V. L. Sushkevich, J. C. Schouten and T. A. Nijhuis, *ChemCatChem*, 2015, **7**, 1161–1176.
- 34 N. M. Wilson and D. W. Flaherty, *J. Am. Chem. Soc.*, 2016, **138**, 574–586.
- 35 A. Pashkova, L. Greiner, U. Krttschil, C. Hofmann and R. Zapf, *Appl. Catal., A*, 2013, **464–465**, 281–287.
- 36 V. R. Choudhary, C. Samanta and T. V. Choudhary, *Appl. Catal., A*, 2006, **308**, 128–133.
- 37 S. Yu, X. Cheng, Y. Wang, B. Xiao, Y. Xing, J. Ren, Y. Lu, H. Li, C. Zhuang and G. Chen, *Nat. Commun.*, 2022, **13**, 4737.
- 38 S. Kanungo, L. van Haandel, E. J. M. Hensen, J. C. Schouten and M. F. Neira d'Angelo, *J. Catal.*, 2019, **370**, 200–209.
- 39 Q. Liu, K. K. Gath, J. C. Bauer, R. E. Schaak and J. H. Lunsford, *Catal. Lett.*, 2009, **132**, 342–348.
- 40 P. Tian, L. Ouyang, X. Xu, J. Xu and Y.-F. Han, *Chin. J. Catal.*, 2013, **34**, 1002–1012.
- 41 J. K. Edwards, S. J. Freakley, A. F. Carley, C. J. Kiely and G. J. Hutchings, *Acc. Chem. Res.*, 2014, **47**, 845–854.
- 42 J. Zhang, P. Tian, A. Xu, L. Ouyang, Z. Yang and J. Xu, *Chin. Chem. Lett.*, 2023, **34**, 108446.
- 43 J. S. Adams, M. L. Kromer, J. Rodriguez-Lopez and D. W. Flaherty, *J. Am. Chem. Soc.*, 2021, **143**, 7940–7957.
- 44 S. J. Freakley, N. Agarwal, R. U. McVicker, S. Althahban, R. J. Lewis, D. J. Morgan, N. Dimitratos, C. J. Kiely and G. J. Hutchings, *Catal. Sci. Technol.*, 2020, **10**, 5935–5944.
- 45 A. Santos, R. J. Lewis, G. Malta, A. G. R. Howe, D. J. Morgan, E. Hampton, P. Gaskin and G. J. Hutchings, *Ind. Eng. Chem. Res.*, 2019, **58**, 12623–12631.
- 46 S. Shaybanizadeh, R. Luque and A. Najafi Chermahini, *Green Chem.*, 2022, **24**, 5524–5534.
- 47 B. E. Solsona, J. K. Edwards, P. Landon, A. F. Carley, A. Herzing, C. J. Kiely and G. J. Hutchings, *Chem. Mater.*, 2006, **18**, 2689–2695.
- 48 N. M. Wilson, P. Priyadarshini, S. Kunz and D. W. Flaherty, *J. Catal.*, 2018, **357**, 163–175.
- 49 T. Ricciardulli, S. Gorthy, J. S. Adams, C. Thompson, A. M. Karim, M. Neurock and D. W. Flaherty, *J. Am. Chem. Soc.*, 2021, **143**, 5445–5464.
- 50 R. J. Lewis, K. Ueura, X. Liu, Y. Fukuta, T. E. Davies, D. J. Morgan, L. Chen, J. Qi, J. Singleton, J. K. Edwards, S. J. Freakley, C. J. Kiely, Y. Yamamoto and G. J. Hutchings, *Science*, 2022, **376**, 615–620.
- 51 R. J. Lewis, K. Ueura, Y. Fukuta, T. E. Davies, D. J. Morgan, C. B. Paris, J. Singleton, J. K. Edwards, S. J. Freakley, Y. Yamamoto and G. J. Hutchings, *Green Chem.*, 2022, **24**, 9496–9507.
- 52 R. J. Lewis, K. Ueura, X. Liu, Y. Fukuta, T. Qin, T. E. Davies, D. J. Morgan, A. Stenner, J. Singleton, J. K. Edwards, S. J. Freakley, C. J. Kiely, L. Chen, Y. Yamamoto and G. J. Hutchings, *ACS Catal.*, 2023, **13**, 1934–1945.
- 53 S. J. Freakley, Q. He, J. H. Harrhy, L. Lu, D. A. Crole, D. J. Morgan, E. N. Ntainjua, J. K. Edwards, A. F. Carley, A. Y. Borisevich, C. J. Kiely and G. J. Hutchings, *Science*, 2016, **351**, 965–968.
- 54 H. C. Li, Q. Wan, C. Du, J. Zhao, F. Li, Y. Zhang, Y. Zheng, M. Chen, K. H. L. Zhang, J. Huang, G. Fu, S. Lin, X. Huang and H. Xiong, *Nat. Commun.*, 2022, **13**, 6072.
- 55 D. Kovačić, R. J. Lewis, C. M. Crombie, D. J. Morgan, T. E. Davies, Á. López-Martín, T. Qin, C. S. Allen, J. K. Edwards, L. Chen, M. S. Skjøth-Rasmussen, X. Liu and G. J. Hutchings, *Green Chem.*, 2023, **25**, 10436–10446.
- 56 Y. Zhang, Q. Sun, G. Guo, Y. Cheng, X. Zhang, H. Ji and X. He, *Chem. Eng. J.*, 2023, **451**, 138867.
- 57 M.-C. Kim, G.-H. Han, X. Xiao, J. Song, J. Hong, E. Jung, H.-K. Kim, J.-P. Ahn, S. S. Han, K.-Y. Lee and T. Yu, *Appl. Surf. Sci.*, 2021, **562**, 150031.
- 58 G. H. Han, X. Xiao, J. Hong, K. J. Lee, S. Park, J. P. Ahn, K. Y. Lee and T. Yu, *ACS Appl. Mater. Interfaces*, 2020, **12**, 6328–6335.
- 59 K. Cao, H. Yang, S. Bai, Y. Xu, C. Yang, Y. Wu, M. Xie, T. Cheng, Q. Shao and X. Huang, *ACS Catal.*, 2021, **11**, 1106–1118.
- 60 V. R. Naina, S. Wang, D. I. Sharapa, M. Zimmermann, M. Hähsler, L. Niebl-Eibenstein, J. Wang, C. Wöll,

- Y. Wang, S. K. Singh, F. Studt and S. Behrens, *ACS Catal.*, 2021, **11**, 2288–2301.
- 61 J. Gu, S. Wang, Z. He, Y. Han and J. Zhang, *Catal. Sci. Technol.*, 2016, **6**, 809–817.
- 62 P. Tian, X. Xu, C. Ao, D. Ding, W. Li, R. Si, W. Tu, J. Xu and Y. F. Han, *ChemSusChem*, 2017, **10**, 3342–3346.
- 63 P. Tian, F. Xuan, D. Ding, Y. Sun, X. Xu, W. Li, R. Si, J. Xu and Y.-F. Han, *J. Catal.*, 2020, **385**, 21–29.
- 64 D. Ding, X. Xu, P. Tian, X. Liu, J. Xu and Y.-F. Han, *Chin. J. Catal.*, 2018, **39**, 673–681.
- 65 S. Wang, R. J. Lewis, D. E. Doronkin, D. J. Morgan, J.-D. Grunwaldt, G. J. Hutchings and S. Behrens, *Catal. Sci. Technol.*, 2020, **10**, 1925–1932.
- 66 M. Zhang, Y. Luo, D. Wu, Q. Li, H. Xu and D. Cheng, *Appl. Catal., A*, 2021, **628**, 118392.
- 67 M. Zhang, H. Xu, Y. Luo, J. Zhu and D. Cheng, *Catal. Sci. Technol.*, 2022, **12**, 5290–5301.
- 68 X. T. Tran, V. L. N. Vo and Y.-M. Chung, *Catal. Today*, 2023, **411–412**, 113821.
- 69 T. Richards, R. J. Lewis, D. J. Morgan and G. J. Hutchings, *Catal. Lett.*, 2022, **153**, 32–40.
- 70 Q. Wu, S. Zhou, C. Fu, J. Zhang, B. Chen, H. Pan and Q. Lin, *New J. Chem.*, 2022, **46**, 8739–8751.
- 71 S. Wang, D. E. Doronkin, M. Hahsler, X. Huang, D. Wang, J. D. Grunwaldt and S. Behrens, *ChemSusChem*, 2020, **13**, 3243–3251.
- 72 T.-T. Huynh, W.-H. Huang, M.-C. Tsai, M. Nugraha, S.-C. Haw, J.-F. Lee, W.-N. Su and B. J. Hwang, *ACS Catal.*, 2021, **11**, 8407–8416.
- 73 D. A. Crole, R. Underhill, J. K. Edwards, G. Shaw, S. J. Freakley, G. J. Hutchings and R. J. Lewis, *Philos. Trans. R. Soc., A*, 2020, **378**, 20200062.
- 74 S. Maity and M. Eswaramoorthy, *J. Mater. Chem. A*, 2016, **4**, 3233–3237.
- 75 S. Wang, K. Gao, W. Li and J. Zhang, *Appl. Catal., A*, 2017, **531**, 89–95.
- 76 W. Wang, W. Xue, F. Yang, J. Li, L. Nie, H. Huang and C. Zhong, *Ind. Eng. Chem. Res.*, 2023, **62**, 11840–11850.
- 77 H. Lee, S. Kim, D.-W. Lee and K.-Y. Lee, *Catal. Commun.*, 2011, **12**, 968–971.
- 78 Y. Liu, Z. Liu, J. Zhang, F.-S. Xiao, X. Cao and L. Wang, *Angew. Chem., Int. Ed.*, 2023, **62**, e202312377.
- 79 Z. Jin, Y. Liu, L. Wang, C. Wang, Z. Wu, Q. Zhu, L. Wang and F.-S. Xiao, *ACS Catal.*, 2021, **11**, 1946–1951.
- 80 Y. Feng, Q. Shao, B. Huang, J. Zhang and X. Huang, *Natl. Sci. Rev.*, 2018, **5**, 895–906.
- 81 P. Liu, Q. Lin, H. Pan, J. Zhao, C. Zhao and Y. Wang, *J. Catal.*, 2019, **377**, 511–523.
- 82 S. Okada, S. Ikurumi, T. Kamegawa, K. Mori and H. Yamashita, *J. Phys. Chem. C*, 2012, **116**, 14360–14367.
- 83 J. Kim, Y.-M. Chung, S.-M. Kang, C.-H. Choi, B.-Y. Kim, Y.-T. Kwon, T. J. Kim, S.-H. Oh and C.-S. Lee, *ACS Catal.*, 2012, **2**, 1042–1048.
- 84 G. M. Lari, B. Puértolas, M. Shahrokhi, N. López and J. Pérez-Ramírez, *Angew. Chem., Int. Ed.*, 2017, **56**, 1775–1779.
- 85 L. F. d. L. e Freitas, B. Puértolas, J. Zhang, B. Wang, A. S. Hoffman, S. R. Bare, J. Pérez-Ramírez, J. W. Medlin and E. Nikolla, *ACS Catal.*, 2020, **10**, 5202–5207.
- 86 R. J. Lewis, M. Koy, M. Macino, M. Das, J. H. Carter, D. J. Morgan, T. E. Davies, J. B. Ernst, S. J. Freakley, F. Glorius and G. J. Hutchings, *J. Am. Chem. Soc.*, 2022, **144**, 15431–15436.
- 87 E. Ye, F. Lin, C. Fu, X. Zhou, Q. Lin, H. Pan and Z. Chen, *ACS Appl. Mater. Interfaces*, 2024, **16**, 27490–27503.
- 88 G. Blanco-Brieva, F. Desmedt, P. Miquel, J. M. Campos-Martin and J. L. G. Fierro, *Catal. Sci. Technol.*, 2020, **10**, 2333–2336.
- 89 H. T. Thuy Vu, V. L. Nam Vo and Y.-M. Chung, *Appl. Catal., A*, 2020, **607**, 117867.
- 90 J. K. Edwards, B. Solsona, E. Ntainjua N, A. F. Carley, A. A. Herzing, C. J. Kiely and G. J. Hutchings, *Science*, 2009, **323**, 1037–1041.
- 91 J. Wu, H. Xu, D. Cao and D. Cheng, *J. Catal.*, 2024, **436**, 115620.
- 92 J. K. Edwards, E. Ntainjua, A. F. Carley, A. A. Herzing, C. J. Kiely and G. J. Hutchings, *Angew. Chem., Int. Ed.*, 2009, **48**, 8512–8515.
- 93 J. K. Edwards, S. F. Parker, J. Pritchard, M. Piccinini, S. J. Freakley, Q. He, A. F. Carley, C. J. Kiely and G. J. Hutchings, *Catal. Sci. Technol.*, 2013, **3**, 812–818.
- 94 R. J. Lewis, E. N. Ntainjua, D. J. Morgan, T. E. Davies, A. F. Carley, S. J. Freakley and G. J. Hutchings, *Catal. Commun.*, 2021, **161**, 106358.
- 95 F. Alotaibi, S. Al-Mayman, M. Alotaibi, J. K. Edwards, R. J. Lewis, R. Alotaibi and G. J. Hutchings, *Catal. Lett.*, 2019, **149**, 998–1006.
- 96 S. Liu, Y. Deng, L. Fu, L. Huang, L. Ouyang and S. Yuan, *ACS Sustainable Chem. Eng.*, 2022, **10**, 3264–3275.
- 97 W. Yan, R. Sun, M. Li, L. Li, Z. Yang, Z. Hua, X. Lu and C. Liu, *Chin. J. Catal.*, 2020, **41**, 312–321.
- 98 C. Ao, P. Tian, L. Ouyang, G. Da, X. Xu, J. Xu and Y.-F. Han, *Catal. Sci. Technol.*, 2016, **6**, 5060–5068.
- 99 L. B. Belykh, N. I. Skripov, T. P. Sterenchuk, E. A. Milenkaya, T. A. Kornaukhova and F. K. Schmidt, *Appl. Catal., A*, 2023, **664**, 119330.
- 100 S. Wang, G. Jiang, Z. Yang, L. Mu, T. Ji, X. Lu and J. Zhu, *ACS Sustainable Chem. Eng.*, 2022, **10**, 13750–13758.
- 101 M. W. Lee, D. Y. Jo, G.-H. Han and K.-Y. Lee, *Catal. Today*, 2022, **397–399**, 232–239.
- 102 X. T. Tran, V. L. N. Vo and Y.-M. Chung, *Mol. Catal.*, 2022, **533**, 112740.
- 103 X. Ji, D. Chen, L. Peng, F. Frison, C. D. Valle, C. Tubaro, M. Zecca, P. Centomo, D. Ye and P. Chen, *Catal. Today*, 2021, **376**, 1–8.
- 104 A. Villa, S. J. Freakley, M. Schiavoni, J. K. Edwards, C. Hammond, G. M. Veith, W. Wang, D. Wang, L. Prati, N. Dimitratos and G. J. Hutchings, *Catal. Sci. Technol.*, 2016, **6**, 694–697.
- 105 Z. Jin, L. Wang, E. Zuidema, K. Mondal, M. Zhang, J. Zhang, C. Wang, X. Meng, H. Yang, C. Mesters and F. S. Xiao, *Science*, 2020, **367**, 193–197.